RSC Advances

PAPER

View Article Online
View Journal | View Issue

Cite this: *RSC Adv.*, 2014, **4**, 44065

Embedded cobalt oxide nano particles on carbon could potentially improve oxygen reduction activity of cobalt phthalocyanine and its application in microbial fuel cells

Jalal Ahmed,[a] Hyung Joo Kim[b] and Sunghyun Kim*[a]

The increasing cost of precious metals, especially platinum, as oxygen reduction catalysts has hindered their widespread use in microbial fuel cells (MFCs). There is an obvious importance for the development of alternative catalysts based on nonprecious metals. Here, we investigated the possibility of cobalt phthalocyanine (CoPc) as an oxygen reduction reaction (ORR) catalyst in an air-cathode MFC. Electrochemical results revealed that cobalt oxide incorporation positively shifted the ORR onset potential of CoPc. Rotating ring-disk experiments confirmed that CoPc exhibited an apparent $4e^-$ reduction pathway in the composite system with minimal hydrogen peroxide production. When applied to MFCs, a maximum power density of 780 mW m^{-2} was achieved with the C-CoOx–CoPc cathode, which was about 50% higher than that with C-CoPc. The voltage output of the MFC dropped only 19% from its initial voltage after 100 days of operation, indicating that our synthesized catalysts are fairly stable over longer operation. The voltage drop partially resulted from the covering of biofilm on the catalyst layer, 89–92% of which was reinstated upon scraping off the biofilm. This work shows that C-CoOx–CoPc could be a potential alternative to Pt in MFCs for sustainable energy generation and a guide to the promising metal oxide-loaded ORR catalyst design.

Received 24th June 2014
Accepted 9th September 2014

DOI: 10.1039/c4ra05940a

www.rsc.org/advances

1. Introduction

A microbial fuel cell is a bioelectrochemical system that can utilize microorganisms as biocatalysts to directly convert a wide variety of organic substances into electricity.[1–3] The electrons produced from the degradation of biomass in the metabolic system of bacteria are directed to the anode and then to the cathode through the external circuit. With a combination of a proper cathodic reaction, electricity is generated. Since MFCs can produce electricity in an environmentally friendly way, they are regarded as an emerging green technology satisfying 'carbon neutral' condition. It has been proven that organic compounds present in various wastes can be effectively degraded while producing electricity.[4] Implementation of MFCs in the treatment system, however, has been limited by significant power reduction when scaled-up and high construction cost.[5] A considerable effort has, therefore, been poured to improve MFC performance by optimizing operational parameters such as electrodes[6,7] surface area, substrate flow rate,[8,9] and temperature.[10,11]

Much effort has also been invested on improving the catalytic activity of ORR catalysts used at cathode as oxygen is considered one of the most suitable electron acceptors in MFCs for its inherent high reduction potential. The fact that no extra energy input is required for oxygen supply to the cathode by passive aeration makes oxygen an ideal cathodic fuel. One of the biggest problems, however, is the slow kinetics of ORR at neutral pHs and at low temperature under whose conditions most MFCs are operated. Although Pt has been known to be the best electrocatalyst for ORR, high cost, easy poisoning, and limited reserve hinder its widespread use as an ORR catalyst. It is estimated that the cost of Pt takes about half of the total capital cost of the fuel cell system. Thus development of suitable catalysts that are free from aforementioned drawbacks while still exhibiting high ORR activity is crucially important. A lot of efforts has been devoted on this subject to replace Pt. Notable among the attempts is the use of transition metal porphyrins and phthalocyanines.[12–15] They have been extensively studied as an alternative to Pt in conventional fuel cells for decades. Iron phthalocyanine (FePc),[16–18] in particular, has been known to exhibit good oxygen reduction activity. Metallo-phthalocyanines (MPc) are usually supported on carbon materials with high surface area and high electric conductivity, and subject to heat-treatment at high temperatures. This greatly increases catalytic activities not only for oxygen reduction but for other reactions

[a]*Department of Bioscience and Biotechnology, Konkuk University, Seoul 143-701, Korea. E-mail: skim100@konkuk.ac.kr; Fax: +82-2-456-2744; Tel: +82-2-450-3378*
[b]*Department of Microbial Engineering, Konkuk University, Seoul 143-701, Korea*

and chemical stability.[19] π–π interaction between π electrons of a phthalocyanine ring and graphitic structure formed by heat treatment has been known to lead to efficient charge transport in the composite system.[20] Delocalized electron density and charge transfer across the metal–carbon interface accelerate ORR process. Also it was confirmed from density functional theory (DFT) that the formation of M–N (M = Fe, Co) cluster at the edge of graphitic pores is energetically feasible and ORR is favored.[21] Catalytic activity is also largely affected by the kind of supporting materials. For example, FePc supported on polyaniline or amino-functionalized carbon nanotube showed improved catalytic activity toward ORR, and as a result led to the higher power density when applied to MFCs.[22,23] Enhanced activity was believed to be resulted from the synergetic effect of phthalocyanine and the supporting materials. Bimetallic systems comprised of non-platinum metals have also shown high ORR activities from synergistic interactions between components.[24–26] Fernandez *et al.*[26] setup a model explaining this phenomenon in which one metal atom breaks O–O bond and another metal reduces thus formed adsorbed oxygen atoms.

Metal–nitrogen–carbon systems came under comprehensive research after Jasinski has discovered that cobalt phthalocyanine (CoPc) catalyzed the oxygen reduction.[27] However, CoPc was proven impractical because of an undesirable two-electron reaction leading to H_2O_2 formation. Notable is that the ability of cobalt oxide (CoOx) to enhance oxygen reduction activity when integrated into the body of the main catalyst such as MnO_2 and Au. Mahmoud *et al.*[28] reported that spinel Mn–Co oxide structure enhanced oxygen adsorption and electron acceptance on the catalyst surface, thus leading to the high ORR activity. In the meantime, Lin *et al.*[29] showed that Au/CoOx binary system changed the oxygen reduction to the four-electron reduction pathway at a very low Co content. At higher Co contents, oxygen reduction proceeded through two- and four-electron pathways in which produced hydrogen peroxide underwent disproportionation by the Co sites. Recently, Goubert-Renaudin and coworkers[30] reported that the catalytic activity of cobalt porphyrin could also be enhanced by integrating metal oxides. Among tested metal oxides, CoOx showed highest ORR activity. It was inferred that the surface of transition metal oxides favored electron localization over the bulk itinerant electron state, which favored the ORR activity. In our previous study, we reported that CoOx-integrated FePc showed better performance than FePc only.[18] But it was not completely understood whether the synergistic effect arise from co-operative Co site or disproportionation of H_2O_2 at high over-potential.

In this work, we synthesized a C-CoOx–CoPc nano-hybrid system as a possible cathode in MFCs. Electrochemical experiments were conducted to understand the role of CoOx for the instantaneous breakdown of H_2O_2. Rotating ring-disk electrode (RRDE) measurements were employed to monitor the effect of embedded CoOx in the hybrid system for its possible decomposing activity of H_2O_2 to water and oxygen. Carbon cobalt oxide (C-CoOx) precursor was first prepared by thermal decomposition of metal compound and carbon powder, and then C-CoOx–CoPc was synthesized by adsorbing CoPc onto the C-CoOx. This hybrid system was then applied to the MFC cathode as a possible alternative to precious metals for an oxygen reduction reaction.

2. Experimental section

2.1. Synthesis of carbon supported cobalt oxide–cobalt phthalocyanine composite

Cobalt nitrate hexahydrate $[Co(NO_3)_2 \cdot 6H_2O]$ was crushed to fine powder in a mortar, to which carbon powder (Vulcan XC-72, Cabot, USA) was added at a ratio that gave 20 wt% of Co with respect to the carbon particles. The resulting composite was placed in a porcelain heating pot, transferred in a furnace and temperature was raised to 110 °C. The sample was kept at this temperature for 1 h to ensure the impregnation of cobalt salt into carbon particles with simultaneous water evaporation. The temperature was then elevated to 400 °C for 1 h at an ambient condition for graphitic structural rearrangement of carbon otherwise disordered[31] and for the formation of cobalt oxide. Thus formed C-CoOx was cooled down to room temperature. 20 mg of CoPc was dissolved in 20 mL of chloroform to which 200 mg of C-CoOx was dissolved so that 0.1 mg CoPc was loaded for each milligram of C-CoOx. The composite was stirred for 4 h under argon gas and filtered under vacuum when supernatant became colorless, and then the filtered sample was rinsed with chloroform and dried at 30 °C.

2.2. Physical characterization

X-ray photoelectron spectroscopic (XPS) measurements were carried out in AXIS Nova (Kratos Inc. UK) with hemispherical energy analyzer using monochromatic light (AlKα source). Samples were finely dispersed on a copper tape. X-ray diffraction (XRD) data were recorded in a Rigaku D/MAX-2500/PC diffractometer using Cu-Kα radiation at 150 kV and 40 mA current. Transmission electron microscopy (TEM) images were taken in a FE TEM (JEM2100F TEM, JEOL Ltd. Japan). Samples were sonicated in ethanol to homogeneous dispersion before being spread on a copper grid (Lacey F/C grid, 300 mesh, 01883-F, Ted Pella Inc. Sweden) and dried under vacuum before placed in the measurement chamber.

2.3. Electrochemical measurements

The ORR activity of synthesized composite material was tested by cyclic voltammetry (CV) on a glassy carbon (GC) electrode in a three-electrode setup using a potentiostat (Autolab PGSTAT 30, ECO CHEM, Netherlands). 2 mg of C-CoOx–CoPc was dispersed in 0.95 mL ethanol followed by the addition of 0.05 mL of 5% nafion solution and subject to sonication. From the resulting catalyst ink, 10 μL ink approximately 81 μg cm^{-2} was applied to the glassy carbon electrode (Pine Instruments, USA) surface (dia. 5.61 mm) by drop-coating. Thus prepared working electrode was dried at 30 °C for 1 h before taking measurements. A Pt wire and a saturated calomel electrode (SCE) were used as a counter and a reference electrode, respectively. For comparison purpose, C-CoPc was prepared and tested in the same way with constant loading amount. Linear sweep voltammetry (LSV) with

a rotating ring-disk electrode (GC disk-GC ring, PINE instrument, USA) was also performed to clearly observe the onset potential of ORR and to obtain details of the ORR mechanism. The GC disk was modified with C-CoPc or C-CoOx–CoPc and the oxygen reduction was performed. The disk electrode potential was scanned over the range in which oxygen was reduced to water while the ring electrode was poised at potential where hydrogen peroxide was oxidized. The RRDE measurements were done in 50 mM phosphate buffer (pH 7.0) at 1600 rpm.

2.4. Construction of MFCs and inoculation of bacteria

MFCs were constructed as described by Cheng and coauthors.[33] A cylindrical shape (3.0 cm φ × 2.0 cm L) reactor with final liquid volume of 14 mL was made of Plexiglas. The anode and cathode distance was kept 2.0 cm. A non wet-proofed carbon cloth (Fuel Cell Earth LLC Inc. type A) and 30% wet-proofed carbon cloth (type B) were used for anode and cathode respectively. The catalyst layer of the air cathode was prepared as previously described.[32] Briefly, 1 mg of synthesized catalyst was mixed with 1 μL of water to make slurry, to which Nafion solution (5%, 7 μL) followed by isopropyl alcohol (2 μL) was added to prepare a homogenous catalyst ink mixture. Thus prepared composite mixture was applied on the solution-faced side of the air cathode diffusion layer and dried overnight at room temperature. 0.5 mg cm^{-2} Pt-C loaded cathode was prepared for the comparison purpose. MFCs were inoculated by mixing 2 mL anaerobic sludge collected from the Jung-Nang sewage plant (Seoul, Korea) with a culture medium. The culture medium consisted of 1 g L^{-1} sodium acetate prepared in 50 mM phosphate buffer containing 12.5 mL L^{-1} minerals and 5 mL L^{-1} vitamins solutions. The MFC was operated in a batch mode with a 1 kΩ external resistance. At least five charging–discharging cycles were conducted to ensure a matured biofilm before collecting data. The polarization curve was then constructed by discharging the cell with external loads of different values using a battery cycler (WBCS300, WonAtech, Korea). Triplicate MFC experiments were conducted and average results were presented.

3. Results and discussion

3.1. Characterization of synthesized C-CoOx–CoPc

The synthesized C-CoOx–CoPc composite was characterized using XPS, XRD, and TEM. Fig. 1 shows the XPS spectra of C-CoOx–CoPc and C-CoOx as a control. A peak at 779 eV appeared for both composite materials characteristic of Co 2p. Only C-CoOx–CoPc shows an N 1s peak at 399.5 eV, indicating that CoPc adsorbed on C-CoOx and nitrogen atoms in a phthalocyanine ring are present. It is also worth mentioning that no peak was observed near 852 eV which is the characteristic binding energy of Co $2p_{3/2}$ for zero valent cobalt suggesting the absence of metallic Co nanoparticles.[34] The presence of O 1s peak at 529.4 eV, which is characteristic of CoO,[35] for both composites indicates that the heat treatment leads to the metallic oxide incorporation but not transforming to the metallic form from the metal salt precursor. XRD patterns of C-CoOx and C-CoOx–

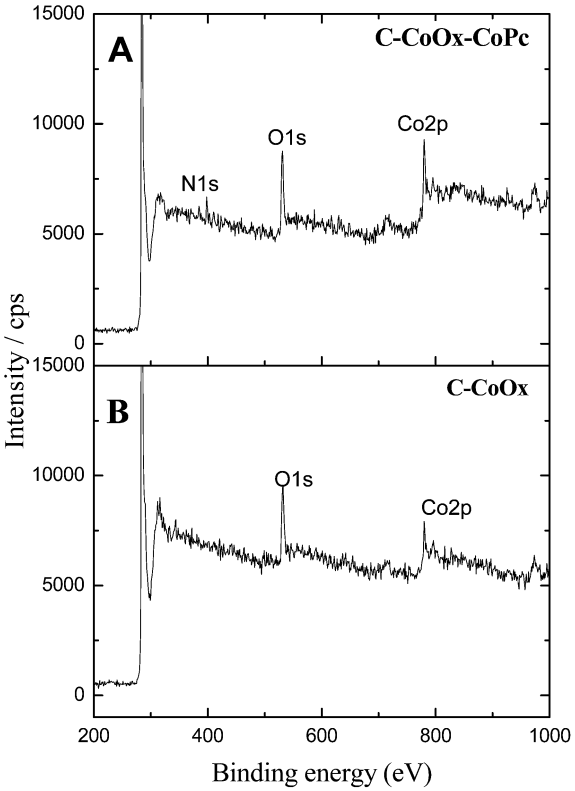

Fig. 1 XPS spectra for C-CoOx–CoPc (A) and C-CoOx (B).

CoPc are shown in Fig. 2. A broad peak of carbon-supported CoPc peak that appears at $2\theta = 8.4°$ is characteristic thin film on carbon.[36] All other peaks are indexed to be a mixture of Co_3O_4 and CoO. Peaks $2\theta = 25.5, 31.2, 36.7, 44.1, 55.6°$ are corresponding to Co_3O_4. Although there are some minor peaks corresponding to CoO, but the dominant crystallite phase is Co_3O_4 supported by other works.[37,38]

Nanoparticle formation of metal oxide was confirmed from the TEM images (Fig. 3). Uniform particles of average size of

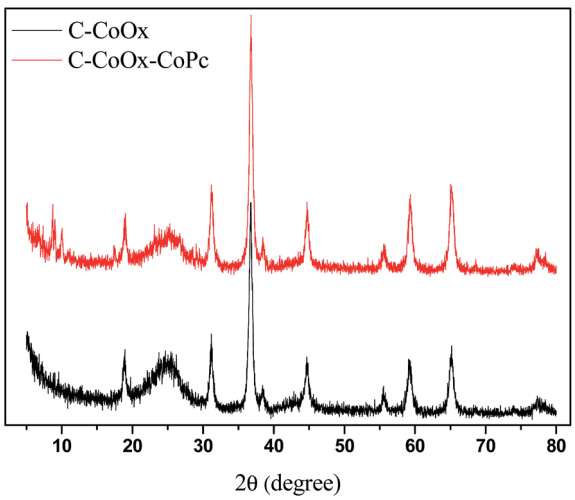

Fig. 2 XRD pattern for C-CoOx (black) and C-CoOx–CoPc (red).

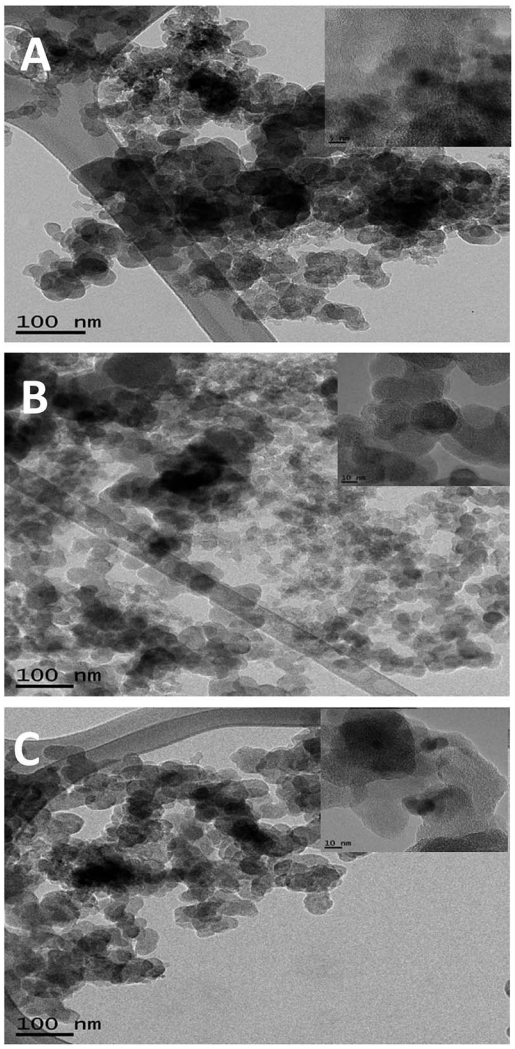

Fig. 3 TEM images of synthesized C-CoOx (A), C-CoPc (B), and C-CoOx–CoPc (C).

30 nm in diameter are homogeneously distributed. The darkest spots surrounded by carbon particles in panel A are attributed to the metallic incorporation inside the carbon structure. Panel B shows the homogeneous dispersion of CoPc on the carbon particles. Panel C is a representative image of C-CoOx–CoPc, which appears with deep dark spots at the center surrounded by light shade (inset). This double spherical nano structure might help to accelerate the charge transfer process and reaction kinetics of ORR due to the higher affinity of CoOx towards oxygen. Moreover, CoOx has specifically been found to catalyze the chemical disproportionation reactions of hydrogen peroxide,[39] an undesirable intermediate formed during the electroreduction of oxygen on the CoPc catalyst surface.

3.2. Electrochemical characterization of C-CoOx–CoPc catalyst

The oxygen reduction activity of C-CoOx–CoPc was analyzed by CV and RRDE and compared with C-CoPc (Fig. 4) to determine how the incorporation of CoOx contributes to the oxygen reduction. From Fig. 3A, it is immediately evident that *ca.* 100 mV ORR potential was decreased for C-CoOx–CoPc, demonstrating a synergistic effect between CoOx and CoPc. Both electrodes show two step oxygen reduction in which oxygen is first reduced to hydrogen peroxide (HO_2^-) and then to water. O_2 reduction to water was also easier at C-CoOx–CoPc than at C-CoOx and C-CoPc. A close inspection of voltammograms reveals an interesting fact: While the two reduction step currents from O_2 to HO_2^- followed by water at C-CoPc are almost identical, the reduction current to HO_2^- from O_2 is larger than that to water from HO_2^- at C-CoOx–CoPc. This strongly implies that some peroxide ions are lost within the electrode.

More insight could be obtained from RRDE experiments (Fig. 4B). From an independent experiment using a GC, we determined hydrogen peroxide oxidation potential at the ring electrode to be 1.2 V *vs.* SCE (data not shown). Being consistent with CV results, the ratio of the current from O_2 to HO_2^- to that from HO_2^- to H_2O is nearly unity at C-CoPc, indicating all the HO_2^- ions are reduced to H_2O. However, the ratio is *ca.* 1.2 at C-CoOx–CoPc. As already pointed out by several authors,[14,40] CoOx promotes ORR activity by disproportionating hydrogen peroxide to oxygen and water. This fact was confirmed by observing ring currents. The ring current began to increase as O_2 reduction is initiated at the disk electrode, and reached the plateau until HO_2^- was reduced to H_2O. In the H_2O formation region, the ring current started to decrease. For C-CoPc, there was only slight decrease whereas a large reduction in current was observed for C-CoOx–CoPc. Tafel plots derived from Fig. 4A are shown in Fig. 4B. Interestingly three electrodes gave the almost identical slope of *ca.* 108 mV per decade in low overpotential region, indicating that a similar ORR mechanism is working. This value is however higher than 60 mV observed in Pt-C catalyst in low overpotential region in strongly alkaline solution.[41] A similar kinetic behavior was observed in manganese oxide nanoparticle ORR catalysts in neutral solutions.[42]

More detailed information as to the oxygen reduction at both electrodes could be obtained by calculating the average number of transferred electrons (n_e) and yield of hydrogen peroxide ($\%HO_2^-$) according to the following equations[37] (Fig. 4C).

$$n_e = \left(\frac{4I_D}{I_D + I_R/N}\right) \quad (1)$$

$$\%HO_2^- = \frac{2I_R/N}{I_D + I_R/N} \times 100 \quad (2)$$

where I_D and I_R are disk and ring currents, respectively. N indicates collection efficiency of the RRDE electrode. In our case N was determined to be 0.37 from an experiment using ferricyanide ion.

The number of electrons involved in ORR at C-CoPc is about 2 in the low overpotential region ($E > -0.15$ V) and rapidly increases as the potential enters the hydrogen peroxide formation region. The constant n_e value of 3.5 was obtained in the potential range of -0.3 and -0.6 V where oxygen is reduced to HO_2^-. This value increases to 3.8 when HO_2^- is further reduced to H_2O at the disk. This result is rather unexpected because the

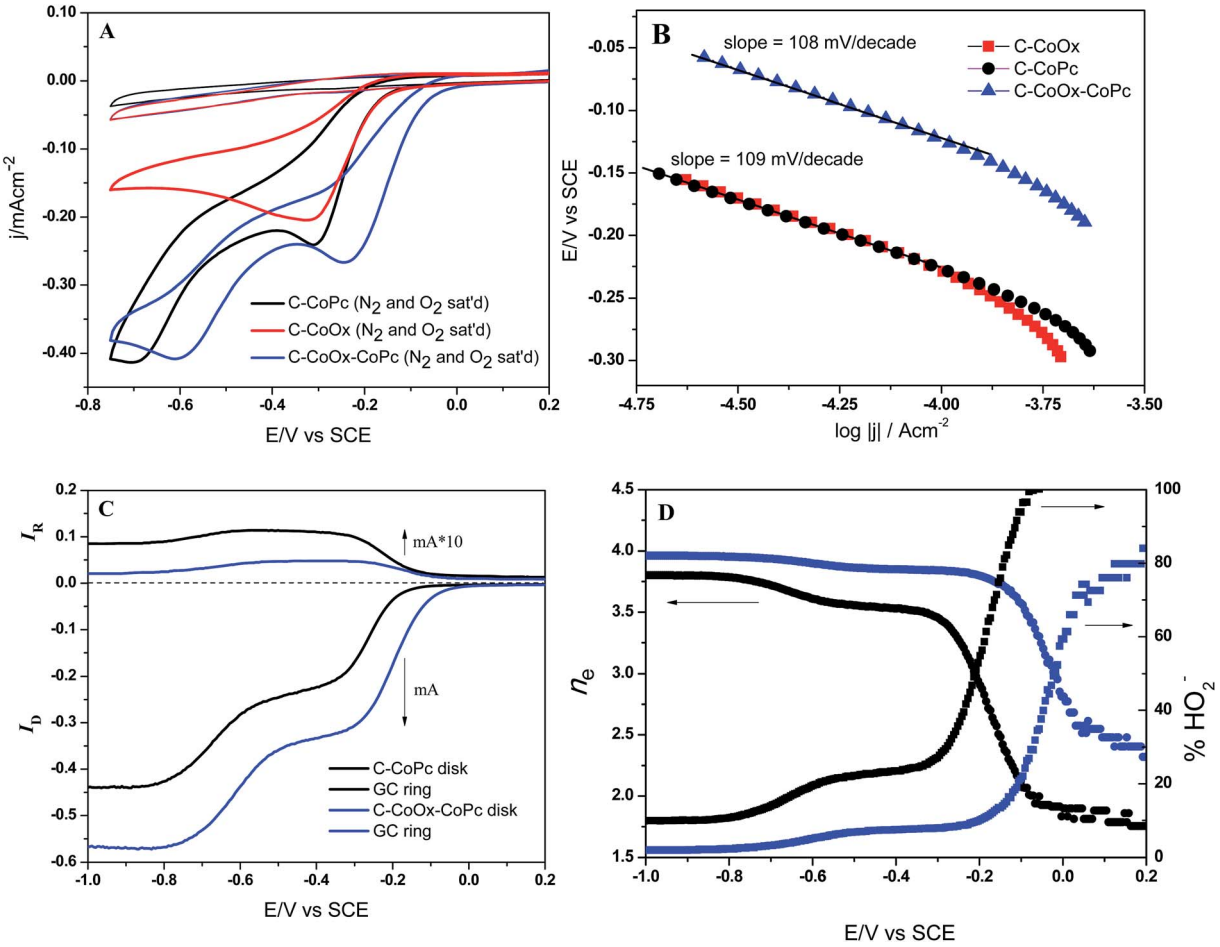

Fig. 4 Panel A: cyclic voltammograms for C-CoPc (black), Co-CoOx (red), and C-CoOx–CoPc (blue) under nitrogen-saturated (thin lines) and oxygen-saturated (thick lines) conditions at 5 mV s^{-1} scan rate. Panel B: Tafel plots for C-CoPc (black), Co-CoOx (red), and C-CoOx–CoPc (blue) in low overpotential region constructed from CV. Panel C: RRDE experiments using a modified GC disk and a GC ring electrode under oxygen-saturated condition at 5 mV s^{-1} scan rate and 1600 rpm. The disk electrode was modified with C-CoPc (black) and C-CoOx–CoPc (blue). The ring potential was set at 1.2 V *vs.* SCE. Panel D: plots of the number of electrons transferred (left) and the percent yield of hydrogen peroxide (right) during the oxygen reduction as a function of potential. All the measurements were done in pH 7 PBS buffer.

voltammogram of the disk electrode clearly shows two steps of reduction of the same magnitude. One possibility is that many of the formed HO_2^- ions are trapped in porous carbon and undergo disproportionation into oxygen and hydroxide ion. And oxygen molecules within the pores are reduced which makes the apparent electron number greater than 2. The percent yield of HO_2^- rapidly drops from almost 100% for the low overpotentials to about 20% in the HO_2^- formation region and further drops to 10% when H_2O is formed, being consistent with changes in n_e values. This study suggests that usual $2e^-$ process taken place on CoPc could instantaneously revert to a $4e^-$ reduction process synergistically.

A similar behavior in n_e and the percent yield of HO_2^- was observed for C-CoOx–CoPc. n_e is less than 3 in the low overpotential region ($E > 0$ V) and increases to over 3.8 in the HO_2^- formation region and further increases to nearly 4.0 when entering the H_2O formation region. This indicates that at C-CoOx–CoPc the reduction product is mostly water whenever hydrogen peroxide is formed. The plot of percent HO_2^- yield also proves this fact. For potentials more negative than −0.2 V, the HO_2^- yield was less than 10%. This apparent $4e^-$ process is attributed to the effective disproportionation of hydrogen peroxide within the C-CoOx–CoPc matrix. As proven by Liu *et al.*,[39] CoOx nanoparticles are probably responsible for this reaction. The fact that higher n_e value and lower HO_2^- yield were resulted from C-CoOx–CoPc than from C-CoPc opens possibility that C-CoOx–CoPc could be applied to MFCs as a cathodic material since hydrogen peroxide causes performance deterioration.

3.3. MFC performance with various cathodes

Five different cathode materials have been applied to MFCs and the MFC performance was tested. Fig. 5A shows the power density plot as a function of current density constructed from polarization curves for different ORR catalyst-loaded air cathodes. The highest power density of 780 ± 38 mW m^{-2} was found with C-CoOx–CoPc among tested cathodes. This result is higher than our previous work with C-CoOx–FePc, although previous catalyst showed better electrochemical ORR performance but

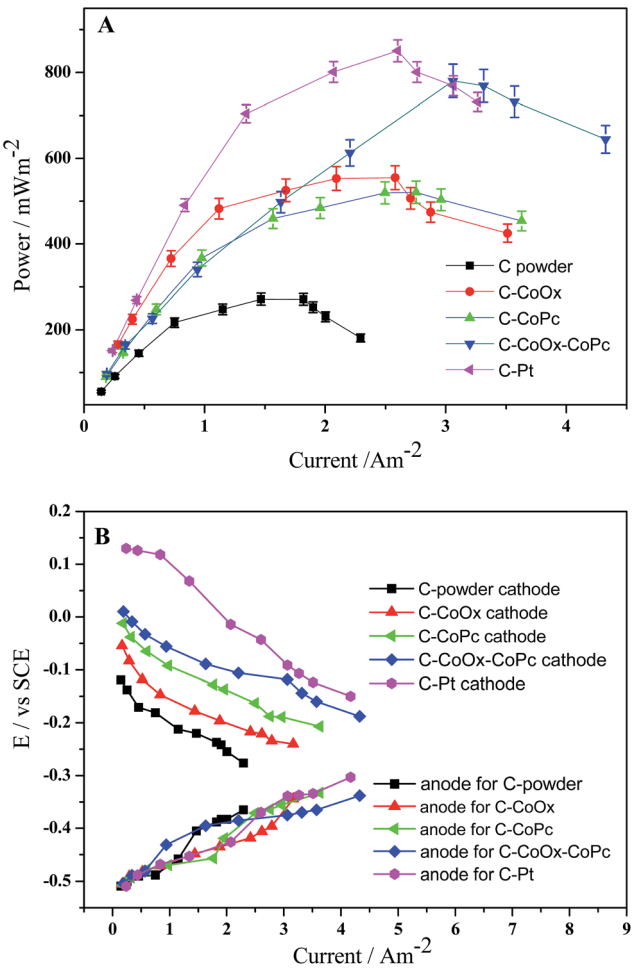

Fig. 5 Panel A: plot of power density *vs.* current density for MFCs constructed with carbon power, C-CoOx, C-CoPc, C-CoOx–CoPc and C-Pt. Panel B: individual electrode potential measured with respect to SCE as a function of current density for each cathode material at 5 mg cm^{-2}.

inferior in MFC performance (654 ± 33 mW m^{-2}). FePc is supposed to degrade and loses active sites when OH^- is adsorbed instead of O_2.[43] Moreover proton transport from MFC anode to cathode is slow process hence cathode microenvironment always maintains a basic condition where FePc is very unstable. Since power density was measured after a stable MFC voltage generation, FePc is deteriorated with this long operation where CoPc is unaffected hence showing higher MFC power density. The MFC with C-CoPc produced only 520 ± 25 mW m^{-2}. Lower power density arises from the fact that produced hydrogen peroxide ions cross over to the anode giving a harmful effect. Carbon powder itself showed a lowest power density (270 mW m^{-2}) as expected. It is noteworthy that appreciable power density (550 ± 27 mW m^{-2}) was observed with C-CoOx cathode, which is comparable to that of C-CoPc. Pt air cathode exhibited best performance producing *ca.* 850 ± 43 mW m^{-2}. However, considering cost and viability, C-CoOx–CoPc is practically more suitable than the Pt cathode.

To verify that different power densities are due to the cathodic limitation, the individual electrode potentials were examined not only for cathodes but for anodes (Fig. 5B). While the anode potential variations with current density were quite similar regardless of cathode materials, a big difference was found for cathode potentials, clearly suggesting that the cathodic reactions govern the MFC performance.

The effect of the catalyst loading amount on the power output has also been examined (Fig. 6). The power density increased with the loading amount and reached maximum value at 5 mg cm^{-2}. Contrary to the expectation, the higher amount did not produce higher power. This might be due to a decrease in oxygen diffusion rate on highly packed surface, which then led to an increase in the diffusion resistance and thus to higher activation overpotential.

Other parameters such as open circuit voltage (OCV) and coulombic efficiency (CE) were also examined for different cathode materials (Table 1). Somehow constant CEs in the range of 21 to 29% were calculated for all five cathodes. This is because they have the same anodic reactions. Noticeable is that the magnitude of OCV reflects the magnitude of the maximum power density. The Pt cathode, which showed the highest maximum power density, gives the highest OCV (820 mV), and the C-CoOx–CoPc cathode shows the second highest OCV (760 mV). Carbon powder, the poorest cathode, gives the lowest OCV (520 mV).

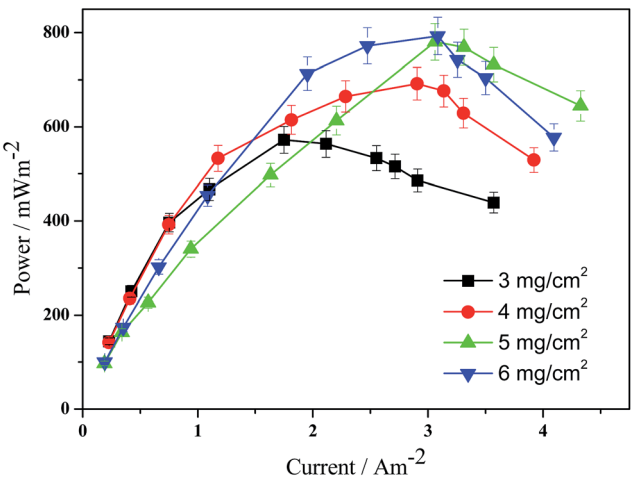

Fig. 6 Effect of the amount of C-CoOx–CoPc applied on the cathode surface on power density as a function of current density.

Table 1 Comparison of MFC performance parameters for various cathode materials

Cathode	OCV (mV ± 10)	P_{max} (mW m^{-2} ± 5%)	CE (% ± 2)
C-Pt	820	850	28
C powder	520	271	21
C-CoOx	670	555	24
C-CoPc	650	519	24
C-CoOx–CoPc	760	780	29

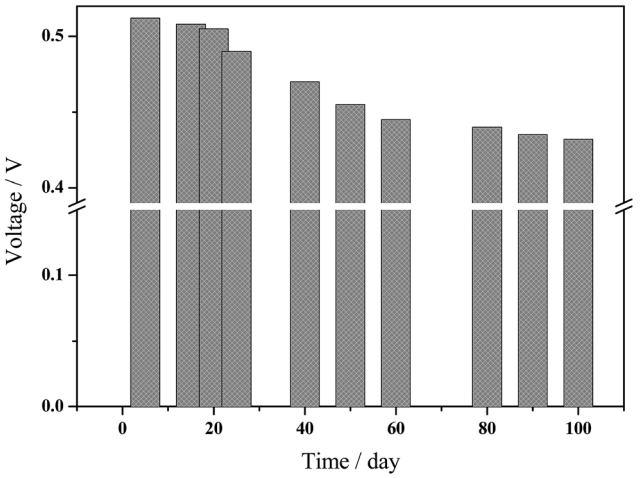

Fig. 7 Variation of output voltage of an MFC with C-CoOx–CoPc cathode under 1 kΩ external load for a long term operation.

3.4. Long term stability

For the practical application, long term stability of MFCs should be warranted. We have subjected MFCs constructed with a C-CoOx–CoPc cathode to full discharging–charging cycles more than 100 days by attaching 1 kΩ external load. The output voltage gradually decreased with time and reached 80% of its initial value after 100 days (Fig. 7). It was also observed that biofilm was formed on the cathode surface, which is typical for single-chamber MFCs.[44] The formation of biofilm on the cathode hinders proton diffusion onto the cathode and thus increases activation overpotential for oxygen reduction. Pores on the surface are clogged with non-conducting biomass that leads to reduction of the number of catalyst active sites. These effects caused by the cathode biofilm therefore decrease voltage output. After removing the biofilm with simple water spray and reassembling the MFC, the output voltage was recovered to 89–92% of its initial value.

4. Conclusions

An inexpensive yet efficient cathode material for oxygen reduction has been developed using cobalt oxide and cobalt phthalocyanine fabricated into the air-cathode single-chamber MFC. The catalyst contained double catalytic spheres where CoPc effectively reduced oxygen to hydrogen peroxide which was readily decomposed by CoOx. RRDE experiments showed that oxygen underwent apparent four-electron reduction through disproportionation of HO_2^- to oxygen and water, this might justify the CoPc as potential candidate for ORR which has not been considered because of its two-electron reduction pathway. As a result, MFCs constructed with C-CoOx–CoPc cathode produced power density of 780 mW m^{-2}, which was 50% higher than that of the catalyst without cobalt oxide component. A biofilm formed on the cathode surface was the main reason that caused a performance drop. Although 19% drop in voltage output was observed after a hundred days of operation, voltage was recovered to 89–92% of the initial value after removing the biofilm. Considering low cost and long term stability, C-CoOx–CoPc can be a potential alternative to Pt in an MFC. We hope that this result opens a window in designing new ORR materials by integrating other suitable metal oxides.

Acknowledgements

This research was supported by the National Research Foundation of Korea (NRF) grant funded by the Korea government (no. 2013R1A2A2A05006503). J. Ahmed gratefully acknowledges financial support from Konkuk University through the Konkuk Brain Pool Program in 2012 and 2013.

References

1 B. E. Logan, B. Hamelers, R. Rozendal, U. Schröder, J. Keller, S. Freguia, P. Aelterman, W. Verstraete and K. Rabaey, *Environ. Sci. Technol.*, 2006, **40**, 5181–5192.
2 U. Schröder, *Phys. Chem. Chem. Phys.*, 2007, **9**, 2619–2629.
3 H. Rismani-Yazdi, S. M. Carver, A. D. Christy and I. H. Tuovinen, *J. Power Sources*, 2008, **180**, 683–694.
4 B. E. Logan, *Water Sci. Technol.*, 2005, **52**, 31–37.
5 K. P. Katuri, P. Kavanagh, S. Rengaraj and D. Leech, *Chem. Commun.*, 2010, **46**, 4758–4760.
6 M. M. Ghangreker and V. B. Shinde, *Bioresour. Technol.*, 2007, **98**, 2879–2885.
7 S. E. Oh and B. E. Logan, *Appl. Microbiol. Biotechnol.*, 2006, **70**, 162–169.
8 I. Ieropoulos, J. Winfield and J. Greenman, *Bioresour. Technol.*, 2010, **101**, 3520–3525.
9 J. Y. Nam, H. W. Kim, K. H. Lim and H. S. Shin, *Bioresour. Technol.*, 2010, **101**, S33–S37.
10 H. Liu, S. A. Cheng and B. E. Logan, *Environ. Sci. Technol.*, 2005, **39**, 5488–5493.
11 S. A. Patil, F. Harnisch, B. Kapadnis and U. Schröder, *Biosens. Bioelectron.*, 2010, **26**, 803–808.
12 K. Wiesener, D. Ohms, V. Neumann and R. Franke, *Mater. Chem. Phys.*, 1989, **22**, 457–475.
13 M. Lefevre, J. P. Dodelet and P. Bertrand, *J. Phys. Chem. B*, 2002, **104**, 11238–11247.
14 K. Scott, A. K. Shukla, C. L. Jackson and W. R. A. Meuleman, *J. Power Sources*, 2004, **126**, 67–75.
15 G. Q. Sun, J. T. Wang and R. F. Savinell, *J. Appl. Electrochem.*, 1998, **28**, 1087–1093.
16 F. Zhao, F. Harnisch, U. Schröder, F. Scholz, P. Bogdanoff and I. Herrmann, *Electrochem. Commun.*, 2005, **7**, 1405–1410.
17 S. Cheng, H. Liu and B. E. Logan, *Environ. Sci. Technol.*, 2006, **40**, 364–369.
18 J. Ahmed, Y. Yuan, L. Zhou and S. Kim, *J. Power Sources*, 2012, **208**, 170–175.
19 B. Y. Baik, G. Kwak and S. Kim, *Bull. Korean Chem. Soc.*, 2006, **27**, 329–332.
20 H. Li, Z. Xu, K. Li, X. Hou, G. Cao, Q. Zhang and Z. Cao, *J. Mater. Chem.*, 2011, **21**, 1181–1186.
21 S. Kattel and G. Wang, *J. Mater. Chem. A*, 2013, **1**, 10790–10797.

22 Y. Yuan, J. Ahmed and S. Kim, *J. Power Sources*, 2011, **196**, 1103–1106.
23 Y. Yuan, B. Zhao, Y. Jeon, S. Zhong, S. Zhou and S. Kim, *Bioresour. Technol.*, 2011, **102**, 5849–5854.
24 O. Savadogo, *Int. J. Hydrogen Energy*, 2002, **27**, 157–169.
25 J. K. Norskov, J. Rossmeisl, A. Logadottir, L. Lindqvist, J. R. Kitchin, T. Bligaard and H. Jonsson, *J. Phys. Chem. B*, 2004, **108**, 17886–17892.
26 J. L. Fernandez, D. A. Walsh and A. J. Bard, *J. Am. Chem. Soc.*, 2005, **127**, 357–365.
27 R. Jasiniski, *Nature*, 1964, **201**, 1212–1213.
28 M. Mahmoud, T. A. Gad-Allah, K. M. El-Khatib and F. El-Gohary, *Bioresour. Technol.*, 2011, **102**, 10459–10464.
29 H. F. Lin, W. Tang, A. Kleiman-Shwarstein and E. W. McFarland, *J. Electrochem. Soc.*, 2008, **155**, B200–B206.
30 N. S. Goubert-Renaudin, X. Zhu and A. Wieckowski, *Electrochem. Commun.*, 2010, **12**, 1457–1461.
31 G. Wu, K. L. More, C. M. Johnston and P. Zelanay, *Science*, 2011, **332**, 443–447.
32 H. Liu and B. E. Logan, *Environ. Sci. Technol.*, 2004, **38**, 4040–4046.
33 S. Cheng, H. Liu and B. E. Logan, *Electrochem. Commun.*, 2006, **8**, 489–494.
34 J. F. Moulder, J. Chastain and R. C. King, *Handbook of X-ray photoelectron spectroscopy: a reference book of standard spectra for identification and interpretation of XPS data*, Physical Electronics, Eden Prairie, MN, 1995.
35 S. C. Petitto, E. M. Marsh, G. A. Carson and M. A. Langell, *J. Mol. Catal. A: Chem.*, 2008, **281**, 49–58.
36 Z. W. Xu, H. J. Li, G. X. Cao, Q. L. Zhang, K. Z. Li and X. N. Zhao, *J. Mol. Catal. A: Chem.*, 2011, **335**, 89–96.
37 R. M. Al-Tuwirqi, A. A. Al-Ghamdi, F. Al-Hazmi, F. Alnowaiser, A. A. Al-Ghamdi, N. A. Aal and F. El-Tantawy, *Superlattices Microstruct.*, 2011, **50**, 437–448.
38 P. R. Shukla, S. Wang, H. Sun, H. M. Ang and T. Moses, *Appl. Catal., B*, 2010, **100**, 529–534.
39 J. Liu, L. H. Jiang, Q. W. Tang, B. S. Zhang, D. S. Su, S. L. Wang and G. Q. Sun, *ChemSusChem*, 2012, **5**, 2315–2318.
40 S. N. S. Goubert-Renaudin, X. L. Zhu and A. Wieckowski, *Electrochem. Commun.*, 2010, **12**, 1457–1461.
41 G. Ma, R. Jia, J. Zhao, Z. Wang, C. Song, S. Jia and Z. Zhu, *J. Phys. Chem. C*, 2011, **115**, 25148–25154.
42 I. Roche and K. Scott, *J. Appl. Electrochem.*, 2009, **39**, 197–204.
43 H. He, Y. K. Lei, C. Xiao, D. R. Chu, R. R. Chen and G. F. Wang, *J. Phys. Chem. C*, 2012, **116**, 16038–16046.
44 J. Ahmed and S. Kim, *Bull. Korean Chem. Soc.*, 2011, **32**, 3726–3729.

